2

Basics of the Photonic Crystal Gratings

Andriy E. Serebryannikov
Hamburg University of Technology, E-3
Germany

1. Introduction

More than twenty years have passed since that time when the analogy between solid-state physics and optics led to the concept of photonic crystals (PCs) (Yablonovitch, 1987). Fast progress in theory and applications of PCs has been stimulated to a large extent by their unique properties that allow increasing the potential of light controlling. Slabs of PC have mainly been studied in case of linear virtual interfaces and a noncurvilinear lattice. A rich variety of the fascinating physical phenomena has been demonstrated for these structures, which include superprism, subwavelength imaging, focusing, collimation, and negative refraction with and without left-handed behaviour (Inoue&Ohtaka, 2004; Luo, 2002). They all appear while using only conventional linear isotropic metals and dielectrics due to the specific dispersion of Floquet-Bloch waves in PCs, which is not obtainable for solid pieces of the same materials. Breaking of periodicity in PCs results in the appearance of defect modes, which manifest themselves in the transmission and waveguide regimes (Joannopoulos, 1995). On the other hand, PCs with curvilinear virtual interfaces but still linear lattice have been investigated in the context of such applications as planoconcave lenses (Gralak, 2000; Vodo, 2005), mirrors (Saado, 2005), and splitters (Wu, 2005). PCs having both curvilinear interfaces and lattice, e.g., coaxial PCs (Schleuer&Yariv, 2004) and atoll resonators (Nojima, 2007) are also known.

New operation regimes can be obtained due to *merging* effects of dispersion and diffraction, e.g., in two-dimensional PCs. In the mid 2000's, PCs with the corrugated interfaces have been proposed to redirect the reflected waves to the side directions (Collardey, 2005), obtain unusual order of the cutoff wavelengths for higher diffraction orders (Serebryannikov, 2006), and realize a new mechanism of negative refraction due to the umklapp refracted beams (Lu, 2007). Later, PCs with the corrugated interfaces have been called *photonic crystal gratings* (PCGs) (Serebryannikov, 2009). Strong asymmetry in transmission has been demonstrated in dielectric two-dimensional PCGs theoretically (Serebryannikov, 2009) and in the microwave experiment (Cakmak, 2010). Recently, a similar effect has been studied in the two-dimensional sonic crystals (Li, 2011). The structures with a corrugated interface and a defect-mode waveguide, which is perpendicular to the interface, have been used for obtaining of the beaming, that is connected with the excitation of surface waves due to corrugations (Caglayan, 2008; Smigaj, 2007). A structure that is excited by a defect-mode waveguide located along the virtual interfaces of the corresponding noncorrugated PC has been suggested (Le Thomas, 2007), where the corrugations provide coupling of an otherwise uncoupled defect mode to an outgoing wave in air.

In this chapter, we focus on the transmission and reflection regimes with strong directional selectivity that appear in PCGs owing to the additional periodic corrugations arranged at the virtual interface(s) of a defect-free slab of PC with linear virtual interfaces and noncurvilinear lattice. First of all, additional corrugations enable downshifting of the frequency range where higher diffraction orders may propagate in air, so that it corresponds to the range of existence of lower-order Floquet-Bloch waves, which are well studied in the context of the above-mentioned phenomena. Theoretical background and numerical results will be presented with the focus on new operation regimes, which can be used in optical devices that require strong directional selectivity. Consideration is restricted here to the two-dimensional square-lattice PCs composed of dielectric rods, while the virtual interfaces of the corresponding noncorrugated PC are assumed to be along Γ-X direction in **k** space, and the incident plane wave is *s*-polarized. Figure 1 illustrates a possible evolution from the slab of PC with the noncorrugated interfaces (a) to the PCG with the one-side (b) and, then, to the PCG with the two-side asymmetric (c) corrugations.

The *first class* of the considered regimes (Sec. 2) includes those related to the unidirectional, i.e., extremely asymmetric transmission. High transmittance from one half-space to the other can be obtained if a PCG is illuminated from the corrugated side, but it is vanishing if illumination is in the opposite direction, within a wide range of the frequency variation (Serebryannikov, 2009). This is probably the most interesting regime obtainable in the dielectric PCGs. Breaking of the spatial inversion symmetry, i.e., introducing nonsymmetry with respect to the midplane of the corresponding noncorrugated PC is required for obtaining of such a forward-backward unidirectional transmission. The necessary condition is that zero diffraction order is not coupled to any Floquet-Bloch wave, but at least one higher diffraction order may propagate in air due to the one-side corrugations. Transmission from the noncorrugated side towards the corrugated side is forbidden, while that from the corrugated side is possible owing to higher diffraction order(s). Single-beam unidirectional deflection and two-beam unidirectional splitting belong to the most typical unidirectional diode-like transmission regimes. The main attention will be paid to the PCs with the noncircular (non-isotropic type) isofrequency dispersion contours (IFCs), which are located in **k** space near either M or X point, and the circular (isotropic type) IFCs, which are located near Γ point and correspond to the effective index of refraction $0<|N_{\mathrm{eff}}|<1$.

The *second class* of the operation regimes (Sec. 3) is connected with the Fabry-Perot type resonances that can appear in the nonsymmetric PCGs so that zero and higher diffraction orders simultaneously contribute to the transmission. Classical resonances, i.e., those with a single (zero) order in transmission, are well known for the noncorrugated slabs of PC (Sakoda, 2001; Serebryannikov, 2010). In the PCGs, strong asymmetry of the Fabry-Perot resonance transmission occurs at normal illumination. It can be obtained even if zero order is only coupled to a Floquet-Bloch wave, despite that the higher orders may also propagate in air due to the one-side corrugations. In this case, the higher orders, which appear at the corrugated exit side and propagate in the exit half-space, can mainly contribute to the transmission, if the PCG is illuminated from the noncorrugated side, but they remain evanescent in the exit half-space, if the PCG is illuminated from the corrugated side. At the same time, a nondominant zero-order transmission is symmetric, i.e., it does not depend on the illumination side.

The *third class* of the operation regimes (Sec. 4) is associated with total reflections that involve at least one higher order. They can be obtained inside a band gap of the PC, if the

corrugated side is illuminated. In turn, only zero order contributes to the reflection, if the noncorrugated side is illuminated, that leads to strong asymmetry. It will be demonstrated that the corrugations enable transformation of a desired part of the incident wave energy into that of higher reflected orders. The presented numerical results are obtained by using the fast coupled integral equation technique (Magath&Serebryannikov, 2005).

2. Unidirectional transmission

Diode is one of the main elements required in various optical and microwave circuits. Obtaining of unidirectional diode-like transmission is usually associated with nonreciprocity and, hence, with the use of anisotropic, e.g., gyromagnetic (Figotin&Vitebskiy, 2001; Yu, 2007; Wang, 2008), or nonlinear (Scalora, 2004; Shadrinov, 2011) materials, that allows breaking time reversal symmetry. Furthermore, spatial inversion symmetry should be broken, i.e., the resulting structure must be nonsymmetric with respect to the midplane similarly to Figs. 1(b) and 1(c). Nonreciprocal transmission can be obtained when the symmetry of the parity-time operator is broken (Rüter, 2010) that can be obtained, for example, in a two-channel structure owing to a proper choice of the real and imaginary parts of the index of refraction.

Various manifestations of directional selectivity in the structures that are reciprocal, because of being made of isotropic linear materials only, but allow asymmetric transmission due to transformation of all or significant part of the incident wave energy into either another polarization or higher diffraction orders, have been a subject of the extensive study for a few years. For example, chiral structures are considered to be perspective for achieving isolation for certain polarization states (Plum, 2009; Singh, 2009). It has recently been demonstrated that the complete optical isolation can be achieved dynamically in a linear photonic system with temporal modulation of the refractive index (Yu&Fan, 2009). Nonmagnetic optical isolators can be obtained in the structures that contain two modulators, in which a desired phase shift appears for the co- and counter-propagating waves due to the temporal modulation of bias voltages (Ibrahim, 2004). In this context, PCGs present another big but yet weakly studied class of the reciprocal structures for asymmetric transmission. Contrary to the chiral structures, neither polarization transformation nor rotation of polarization plane occurs in PCGs at asymmetric transmission, provided that they are made of linear isotropic materials.

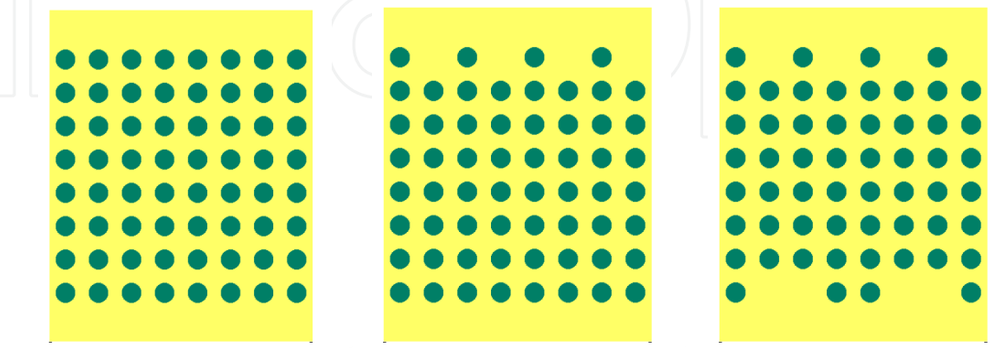

(a) (b) (c)

Fig. 1. Noncorrugated slab of square-lattice PC (a) and the corresponding PCGs which have one-side (b) and two-side (c) corrugations.

2.1 Physical background

First, let us briefly consider the effect of breaking spatial inversion symmetry in the conventional dielectric gratings. In line with the classical theory of diffraction gratings (Petit, 1980), transmission and reflection are characterized in terms of the nth order transmission and reflection efficiencies, which are given by $t_n = |\tau_n|^2$ and $r_n = |\rho_n|^2$ and take into account a part of the incident wave energy in the corresponding propagating orders. Here, τ_n and ρ_n are the nth order transmission and reflection coefficients. In turn, transmittance T and reflectance R are given by a sum over all the orders propagating in air. According to the grating formula (Petit, 1980), the nth order diffraction angle, ϕ_n, is determined from

$$\sin\phi_n = \sin\theta + 2\pi n / kL, \tag{1}$$

where θ is angle of incidence and L is grating period, so that ϕ_n takes a real value for an order that propagates in air. All the diffraction angles for the transmitted beams are measured in the counter-clockwise direction with respect to the normal to the exit side. The angle of incidence is measured in the counter-clockwise direction with respect to the normal to the input side.

Figure 2 presents the transmission spectra for the two nonsymmetric dielectric gratings. One can see that $t_0^{\rightarrow} = t_0^{\leftarrow} = t_0$ but $t_n^{\rightarrow} \neq t_n^{\leftarrow}$ at $|n|=1$, while $\theta = \theta^{\rightarrow} = \theta^{\leftarrow} = 0$, where $\rightarrow$ and $\leftarrow$ stand for the forward (here – from the top) and backward (from the bottom) illumination, respectively. A partially asymmetric transmission with higher orders being responsible for the asymmetry, while the zero-order transmission is symmetric, can be observed in Fig. 2. This is one of the fundamental properties of the nonsymmetric gratings. The ratios $\chi^{\rightarrow} = \sum_{(m\neq 0)} t_m^{\rightarrow} / t_0$ and $\chi^{\leftarrow} = \sum_{(m\neq 0)} t_m^{\leftarrow} / t_0$ may strongly depend on frequency and geometrical and material parameters of the grating. Replacing a dielectric with a PC enables a wide range where $t_0 = 0$ and $t_m^{\leftarrow} = 0$ and, hence, $\chi^{\rightarrow} = \infty$ and $\chi^{\rightarrow} >> \chi^{\leftarrow}$. In the other words, the "*strength" of asymmetry can be enhanced*, so that asymmetric transmission becomes unidirectional, i.e., $T^{\rightarrow} \neq 0$ and $T^{\leftarrow} = 0$. Owing to the band gaps, unidirectional transmission can appear inside wide frequency and incidence angle ranges. This is distinguished from a solid dielectric grating, where these conditions might hypothetically be realized only for a pair of frequency and angle values, but not inside wide ranges. In fact, unidirectional transmission like that in PCGs should not appear in nonsymmetric dielectric gratings, where zero order is always coupled to a wave propagating in the dielectric.

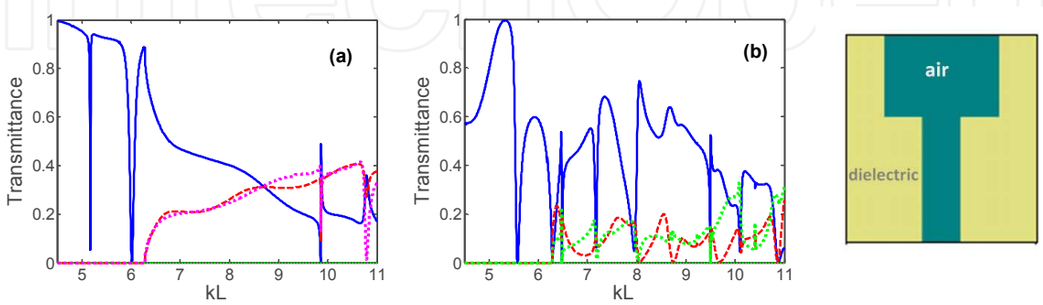

Fig. 2. Transmittance for two nonsymmetric gratings made of dielectric with permittivity (a) $\varepsilon_d = 2.1$ and (b) $\varepsilon_d = 5.8$; solid line - $t_0^{\rightarrow} = t_0^{\leftarrow} = t_0$, dotted line - $t_{\pm 1}^{\rightarrow}$, and dashed line - $t_{\pm 1}^{\leftarrow}$; right panel - geometry of a grating period.

The use of gyromagnetic and nonlinear materials enables unidirectional devices with a single transmission channel like in conventional electronic diodes. Transmission mechanism in the PCGs needs at least two transmission channels, every being associated with a certain in-air propagating order. In the contrast with the nonreciprocal structures that contain anisotropic or nonlinear materials and reciprocal chiral structures, all the diffracted beams in PCGs show the same linear polarization. In line with the previous studies of PCGs (Serebryannikov, 2009), zero order being uncoupled to any Floquet-Bloch wave is required for obtaining of the unidirectional transmission, that in turn dictates the allowed values of θ and IFC shapes. Accordingly, at the corrugated-side illumination, the *umklapp* refractions are only possible.

Two typical coupling scenarios are demonstrated in Fig. 3. Conservation of the wave vector component that is parallel to the interface, k_x, requires that the IFC crosses a construction line, in order to couple the corresponding order to a Floquet-Bloch wave of the PC (Foteinopoulou&Soukoulis, 2005; Lu, 2007). Locations of the construction lines are determined by the following condition:

$$k_x^{(n)} = (\omega / c)\sin\theta + 2\pi n / L . \tag{2}$$

Figures 3(a)-3(c) illustrate the coupling mechanism in case of the simplest, i.e., narrow circular IFCs around Γ point, for which the diffraction relevant unidirectional transmission may appear. They correspond to an isotropic material with the index of refraction $0<N<1$, i.e., are narrower than the IFC in air at the same frequency. Hence, similar asymmetry in transmission can be observed, for example, in the nonsymmetric gratings made of a material with $0<N<1$, e.g., a Drude metal above the plasma frequency, or a wire medium above the effective plasma frequency (Serebryannikov&Ozbay, 2009). Figures 3(d)-3(f) illustrate the coupling mechanism in case of near-square IFCs located around M point, which can be obtained in dielectric PCs. Construction lines are plotted for a value of θ, at which at least one higher diffraction order is coupled to a Floquet-Bloch wave due to the corrugations.

In Figs. 3(a) and 3(d), only zero order may propagate in air regardless of whether the incidence is forward or backward. This case is assumed to correspond to a noncorrugated slab of PC, as in Fig. 1(a), or to a PCG in the frequency range where all higher orders are evanescent. In Figs. 3(b) and 3(e), the first order(s) may propagate in air and is allowed to couple to the Floquet-Bloch wave, for the corrugated-side illumination, but should remain evanescent in the input half-space and uncoupled to the Floquet-Bloch wave at the noncorrugated-side illumination. Thus, transmission is not vanishing in the former case only. Assuming that we initially have a noncorrugated slab of PC like that in Fig. 1(a), and then removing some rods from one of the interface layers, we obtain a PCG like that in Fig. 1(b), which is nonsymmetric with respect to the midplane. The simplest corrugations can be obtained by removing every second rod from an interface layer, so that the lateral period of the PCG is $L=2a$, where a is PC lattice constant. In Figs. 3(b) and 3(e), it is assumed that $P=2$ is the minimal integer value of P in $L=Pa$, which provides such a location of the construction lines with respect to the IFC at a given frequency that unidirectional transmission can be obtained. In fact, P depends on the concrete performance of PCG and, thus, may be a rather arbitrary integer. A PCG can still be nonsymmetric and, thus, might support asymmetric transmission, while having corrugations at the both sides, e.g., see Fig. 1(c). However, a larger difference between the periods of the two interfaces should provide a stronger

asymmetry in terms of the number of the orders contributing to the transmission. In order to obtain unidirectional transmission with rather strong forward and zero backward transmission, the value of a must be chosen so that higher diffraction orders may not propagate due to the effect of the noncorrugated interface. In Figs. 3(c) and 3(f), the same IFCs are presented as in Figs. 3(b) and 3(e), respectively, but now $L = 4a$. Hence, the distance between the neighbouring construction lines is reduced by factor of 2. As a result, now more diffraction orders may propagate in air due to the corrugated interface, and more orders among them may be unidirectionally coupled to a Floquet-Bloch wave.

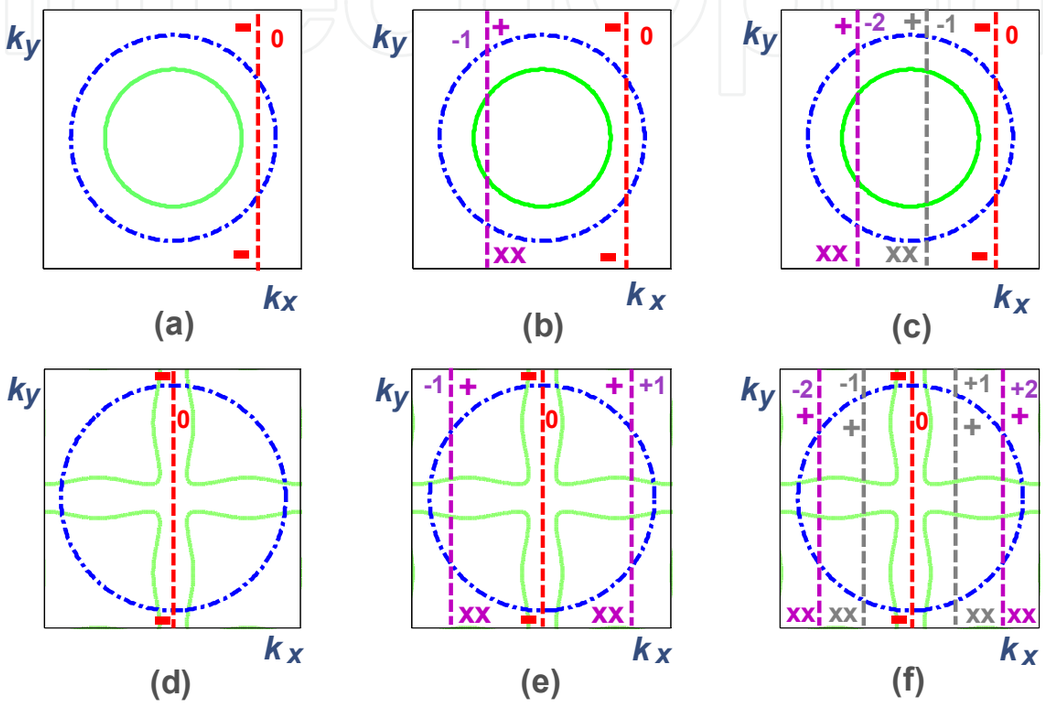

Fig. 3. Coupling scenarios leading to unidirectional transmission: green solid line - IFC of PC; blue dash-dotted circle - IFC in air; dashed lines - construction lines; ″0″ , ″-1″, ″+1″, ″-2″ and ″+2″ denote the order index (n); ″+″ and ″-″ at plot top indicate that the corresponding order is either coupled or not coupled to a Floquet-Bloch wave, if the corrugated side is illuminated; ″-″ and ″xx″ at plot bottom indicate that the corresponding order is either uncoupled at the noncorrugated interface or does not propagate in the input half-space, at the noncorrugated-side illumination; IFCs of PC are assumed to be located around (a-c) Γ point and (d-f) M point; plots (a,d): noncorrugated slab of PC, L=a; plots (b,e): PCG with the simplest one-side corrugations, L=2a; plots (c,f): PCG with the one-side corrugations, L=4a.

From this consideration, it is clearly seen why at least the first negative order for positive nonzero θ and the first positive and first negative orders for zero θ must propagate in air and be coupled to a Floquet-Bloch wave. The scenario shown in Fig. 3(b) corresponds to the regime of *single-beam unidirectional deflection*. The angle between the directions of the incident and single transmitted beams is given by $\Omega=\theta-\phi_{-1}$. At a larger number of the orders propagating in air, as in Fig. 3(c), there may be multiple open transmission channels, every being connected with a certain order, so that splitting occurs in the unidirectional

deflection regime. In the general case, we have $t_n \neq t_m$ and $\phi_n \neq \phi_m$, $n \neq m$, for all the propagating orders. In the situation shown in Fig. 3(e) for θ=0, two beams are allowed to propagate in air, $t_{+1} = t_{-1} \neq 0$ and $\phi_{+1} = -\phi_{-1}$. The number of the transmitted beams at normal incidence is always even, since they propagate symmetrically with respect to the normal, $t_{+n} = t_{-n}$ and $\phi_{+n} = -\phi_{-n}$. Thus, *two-beam unidirectional splitting* appears in this case, while deflection of the beams with n=m and n=-m is symmetric regarding the normal. It is noteworthy that the IFC shapes, which can be obtained in two-dimensional PCs but are distinguished from those in Fig. 3, can also be consistent with the requirements to the diffraction relevant mechanism of unidirectional transmission (Serebryannikov, 2009). Furthermore, this remains true for IFCs that are typical for one-dimensional PCs (Kang, 2010) and anticutoff (indefinite) media (Schurig&Smith, 2003). Hence, this mechanism is quite flexible regarding the choice of materials/structures that might be utilized to create a nonsymmetric grating.

Since the structures we consider are assumed to be composed of isotropic linear materials only, transmission remains reciprocal in sense of the Lorentz Lemma (Kong, 2005). This results in the equal transmittances while replacing source and observation point with each other, i.e., (i) when the PCG is illuminated from the corrugated side at θ=$\theta^{\rightarrow}$ and (ii) when the PCG is illuminated from the noncorrugated side but at $\theta = \theta^{\leftarrow} = \phi_n^{\rightarrow}$, where $\phi_n^{\rightarrow}$ is the diffraction angle for the nth order transmitted beam at the corrugated-side illumination. For example, if the beam of the order n=-1 is the only higher-order propagating beam, as can appear at nonzero θ, and $T^{\rightarrow} = t_{-1}^{\rightarrow} \approx \tilde{T}$ at θ=$\theta^{\rightarrow}$, then $T^{\leftarrow} = t_{-1}^{\leftarrow} \approx \tilde{T}$ at θ=$\theta^{\leftarrow} = \phi_{-1}^{\rightarrow}$. This does not contradict with the fact that the transmission is unidirectional for the two *opposite* directions of incidence.

2.2 Asymmetry in threshold location

In the conventional dielectric gratings, each higher order ($|n|$>0) has a cutoff wavelength and, hence, a threshold frequency, i.e., it propagates if

$$k > |\alpha_0 + 2\pi n / L|, \tag{3}$$

where $\alpha_0 = k \sin\theta$, k=ω/c (Petit, 1980). In the gratings made of Drude metals or composites, the actual thresholds have different locations as compared to the classical case that is associated with dielectric gratings (Serebryannikov & Ozbay, 2009). In the PCGs with either dielectric or metallic rods, the actual thresholds can also be affected by location of the stop bands of the PC (Serebryannikov, 2006; Serebryannikov, 2009).

Let denote the k thresholds which correspond to the boundary between the propagation and evanescent regimes for the nth diffraction order in a dielectric grating by

$$k_{\pm n} = 2\pi n / [L(1 \mp \sin\theta)], \tag{4}$$

where $n \geq 0$ and $\theta \geq 0$. In the vicinity of k=$k_{\pm n}$, rapid variations in t_n and r_n often appear, which are assigned to the Rayleigh-Wood anomalies (Hessel&Oliner,1965). In turn, the actual thresholds for a PCG with one-side corrugations at the exit interface are denoted by $\tilde{k}_n^{(S)}$. The actual thresholds for a PCG with one-side corrugations at the input interface are

denoted by $\hat{k}_n^{(S)}$. Here, S=T for transmission and S=R for reflection. Finally, $k^{(u)}$ and $k^{(l)}$ denote k values that correspond to the upper and lower boundaries of the first stop band. Figure 4 schematically shows the stop and pass bands, the idealized transmission spectrum of PC, the threshold values of k, and the ranges of propagation of the lowest higher order(s) in transmission, for the both PCG and dielectric grating with one-side corrugations. According to Fig. 4(a),

$$k^{(l)} < k_m < k^{(u)} = \tilde{k}_m^{(T)}, \tag{5}$$

where m=-1 if $\theta \neq 0$ and $m = \pm 1$ if $\theta = 0$. In this case, location of the actual cutoff is determined by the upper boundary of the stop band. The mth order(s) propagate in the exit half-space due to the corrugated interface, starting from this boundary. In Fig. 4(b),

$$k^{(l)} < k_m < k^{(u)} < \hat{k}_m^{(T)}. \tag{6}$$

Hence,

$$\tilde{k}_m^{(T)} \neq \hat{k}_m^{(T)}, \tag{7}$$

that is distinguished from the classical grating theory, which gives

$$\tilde{k}_m^{(T)} = \hat{k}_m^{(T)}. \tag{8}$$

The situation in Fig. 4 is realized if zero order is only coupled to the second lowest Floquet-Bloch wave of the PC, i.e., at $k^{(u)} < k < \hat{k}_m^{(T)}$, leading to that $t_0^{\rightarrow} = t_0^{\leftarrow}$ and $T^{\rightarrow} = t_0^{\rightarrow}$ while $T^{\leftarrow} > t_0^{\leftarrow}$. In fact, $\hat{k}_m^{(T)}$ is determined in Fig. 4(b) by the lower boundary of the third lowest passband, for which the mth order(s) are assumed to be coupled to the Floquet-Bloch wave.

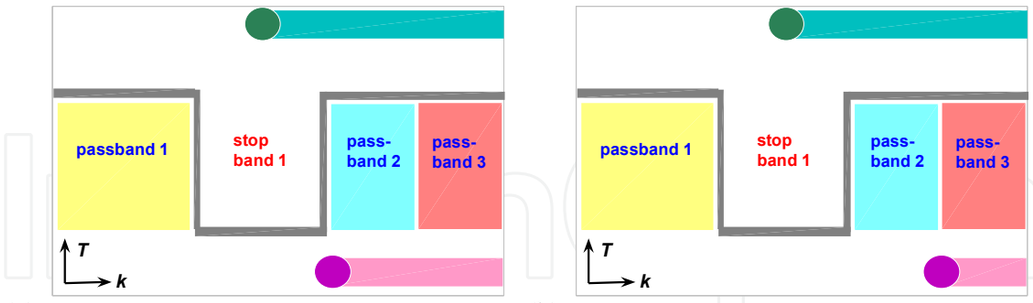

(a) (b)

Fig. 4. Example of composition of pass and stop bands of PC that affects k-domain threshold of higher order(s) in case when $k_m < k^{(u)}$; circles – the actual thresholds in transmission for the dielectric grating (top) and PCG (bottom); the adjacent rectangles show the k ranges where the mth order(s) may propagate; gray line – the idealized transmission spectrum; plot (a) – noncorrugated-side illumination, plot (b) – corrugated-side illumination.

Figure 5 schematically shows the stop and pass bands of the PC and reflection spectrum together with the thresholds and ranges of contribution of the lowest higher order(s) in reflection for the both PCG and dielectric grating with one-side corrugations. In Fig. 5(a), we

have $k_m < k^{(u)} < \tilde{k}_m^{(R)}$ where m is the same as in Fig. 4. Thus, location of the actual threshold is determined here by the lower edge of the third lowest passband, i.e., $\tilde{k}_m^{(R)} = \hat{k}_m^{(T)}$. In turn, $\tilde{k}_m^{(T)} \neq \tilde{k}_m^{(R)}$. In Fig. 5(b), $\hat{k}_m^{(R)} = k_m$, as in the dielectric grating case. Then, $\hat{k}_m^{(R)} \neq \tilde{k}_m^{(R)}$, $\hat{k}_m^{(T)} \neq \hat{k}_m^{(R)}$, and $\tilde{k}_m^{(T)} \neq \hat{k}_m^{(R)}$. Hence, in the contrast with nonsymmetric dielectric gratings, asymmetry in threshold location may appear owing to peculiar types of PC dispersion. In fact, the difference in location of the ranges of $t_m^{\rightarrow} = 0$ and $t_m^{\leftarrow} = 0$, on the one hand, and $r_m^{\rightarrow} = 0$ and $r_m^{\leftarrow} = 0$, on the other hand, is a key feature that is connected with the expected asymmetry in transmission and reflection at least for lower-order stop and pass bands. For higher-order bands, it can be explained in terms of the generalized cutoffs/thresholds.

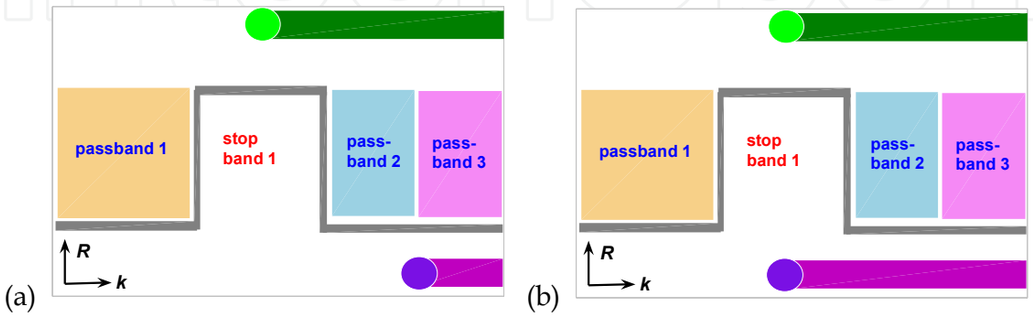

Fig. 5. Same as Fig. 4 but for reflection.

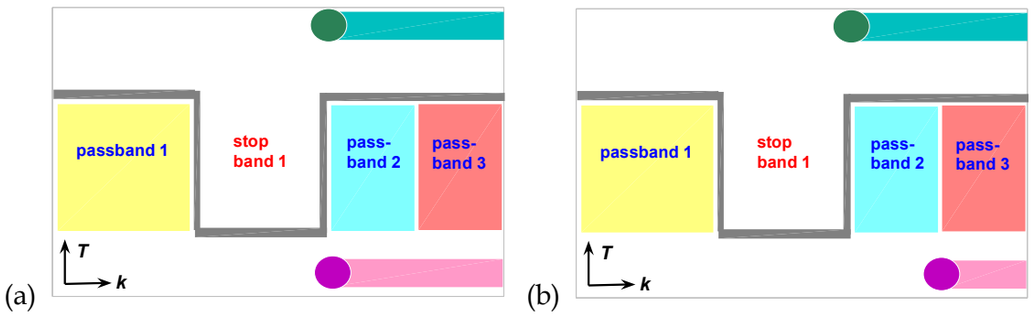

Fig. 6. Same as Fig. 4 but in case when $k_m = k^{(u)}$.

Figures 6 and 7 are analogous to Figs. 4 and 5, respectively, but now $k_m = k^{(u)}$. In the contrast with Figs. 4 and 5, we have simultaneously $\hat{k}_m^{(T)} = \tilde{k}_m^{(R)} > k_m$ and $\tilde{k}_m^{(T)} = \hat{k}_m^{(R)} = k_m$. In turn, $\tilde{k}_m^{(T)} \neq \hat{k}_m^{(T)}$ and $\tilde{k}_m^{(R)} \neq \hat{k}_m^{(R)}$. Hence, the different combinations of locations of $\tilde{k}_m^{(S)}$ and $\hat{k}_m^{(S)}$ with respect to each other and to k_m can be obtained by adjusting the corrugation and PC lattice parameters.

2.3 Forward vs backward transmission

Let us consider the effect of variation in L on the appearance of higher orders in the transmission, in both cases of the corrugated-side and the noncorrugated-side illumination, at normal incidence. An example is shown in Fig. 8 for typical values of the rod-diameter-to-lattice-constant ratio, d/a, relative permittivity of the rod material, ε_r, and an intermediate number of the rod layers, Q. Figures 8(a) and 8(b) partially correspond to the case of the k thresholds location, as in Figs. 5(a) and 5(b).

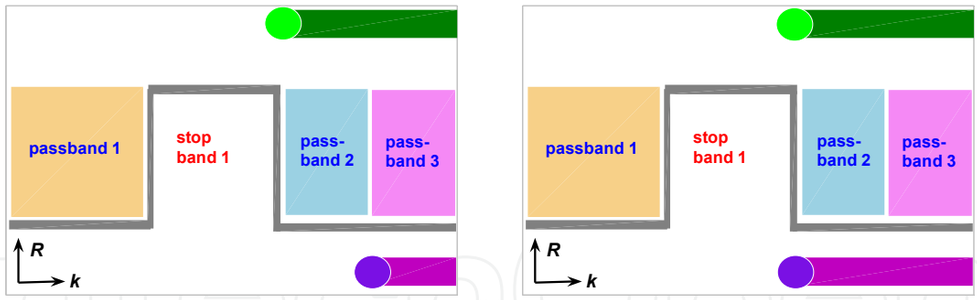

(a) (b)

Fig. 7. Same as Fig. 5 but in case when $k_m = k^{(u)}$.

Indeed, $T^{\rightarrow} = t_0$ but $T^{\leftarrow} = t_0 + t_{-1}^{\leftarrow} + t_{+1}^{\leftarrow}$ at 6<*kL*<8.4. At the same time, $T^{\rightarrow} = t_{-1}^{\rightarrow} + t_{+1}^{\rightarrow}$ and $T^{\leftarrow} = 0$ at 8.4<*kL*<10.5, where $\phi_{\pm 1}$ is varied from ± 48 to ± 37 degrees. In fact, the difference between these two cases originates from the different locations and shapes of IFCs. For the first of them, which corresponds to the second lowest Floquet-Bloch mode, the IFCs are located around Γ point, but narrower than in air. Thus, the orders with $n = \pm 1$ may propagate in air due to the corrugated interface, but are not coupled. For the second of them, which corresponds to the third lowest Floquet-Bloch mode, the IFCs are located around M point, so that the orders with $n = \pm 1$ may propagate in air due to the corrugations and are coupled at the corrugated-side illumination. In turn, zero order is not coupled.

In the first range, we observe *one-way transmission* with the both symmetric (t_0) and asymmetric (t_n, $|n|>0$) components being nonzero. This case is similar to that demonstrated for the nonsymmetric microwave metallic gratings, where different periods at the two sides are created by a proper branching of the thin slit waveguides (Lockyear, 2006), and in the nonsymmetric gratings that contain the Drude material layers, while the periods are different owing to the one-side corrugations (Serebryannikov&Ozbay, 2009). In all the figures, the most representative ranges with $T^{\rightarrow} = t_0$ and $T^{\leftarrow} > t_0$ are denoted by "One-Way". In the second range, *unidirectional transmission* takes place in the form of unidirectional splitting, i.e., $t_{-1}^{\rightarrow} = t_{+1}^{\rightarrow}$, $T^{\rightarrow} = t_{-1}^{\rightarrow} + t_{+1}^{\rightarrow}$, while $T^{\leftarrow} = 0$. In Figs. 8(a) and 8(b), one more range of unidirectional splitting is seen at 11.2<*kL*<12.4, where $\varphi_{\pm 1}$ is varied from ± 34 to ± 30 degrees. It is connected with the fifth lowest Floquet-Bloch mode. Here, we again have $T^{\rightarrow} \neq 0$ and $T^{\leftarrow} = 0$, while even a higher transmittance is achieved than at 8.4<*kL*<10.5. Furthermore, $T^{\rightarrow} = 1$ at the lower edge of the passband, so that exactly the diode regime is realized. In the figures, the most representative ranges of unidirectional transmission ($T^{\rightarrow} \neq 0$ and $T^{\leftarrow} = 0$) are denoted by "UD".

Increasing the number of the rod columns per grating period might lead to that the actual thresholds are shifted towards smaller *ka* and, hence, lower passbands. An example is shown in Figs. 8(c) and 8(d) at *P*=3. Contrary to the case of *P*=2, $t_{+n} \neq t_{-n}$ at $|n|>0$. Unidirectional transmission with $T^{\rightarrow} = t_{-1}^{\rightarrow} + t_{+1}^{\rightarrow}$ and $T^{\leftarrow} = 0$ appears already for the lowest Floquet-Bloch mode, i.e., at the edge of the lowest passband for 7<*kL*<7.9, where ϕ_{-1} is varied from -63.8 to -52.7 degrees. The IFCs are located now around M point, so that zero order is uncoupled. In turn, at smaller *kL*, the IFCs are located around Γ point that enables coupling of zero order. For the third lowest Floquet-Bloch mode, we obtain unidirectional transmission with $T^{\rightarrow} = t_{-1}^{\rightarrow} + t_{+1}^{\rightarrow} + t_{-2}^{\rightarrow} + t_{+2}^{\rightarrow}$ and $T^{\leftarrow} = 0$ at 13.2<*kL*<15.8.

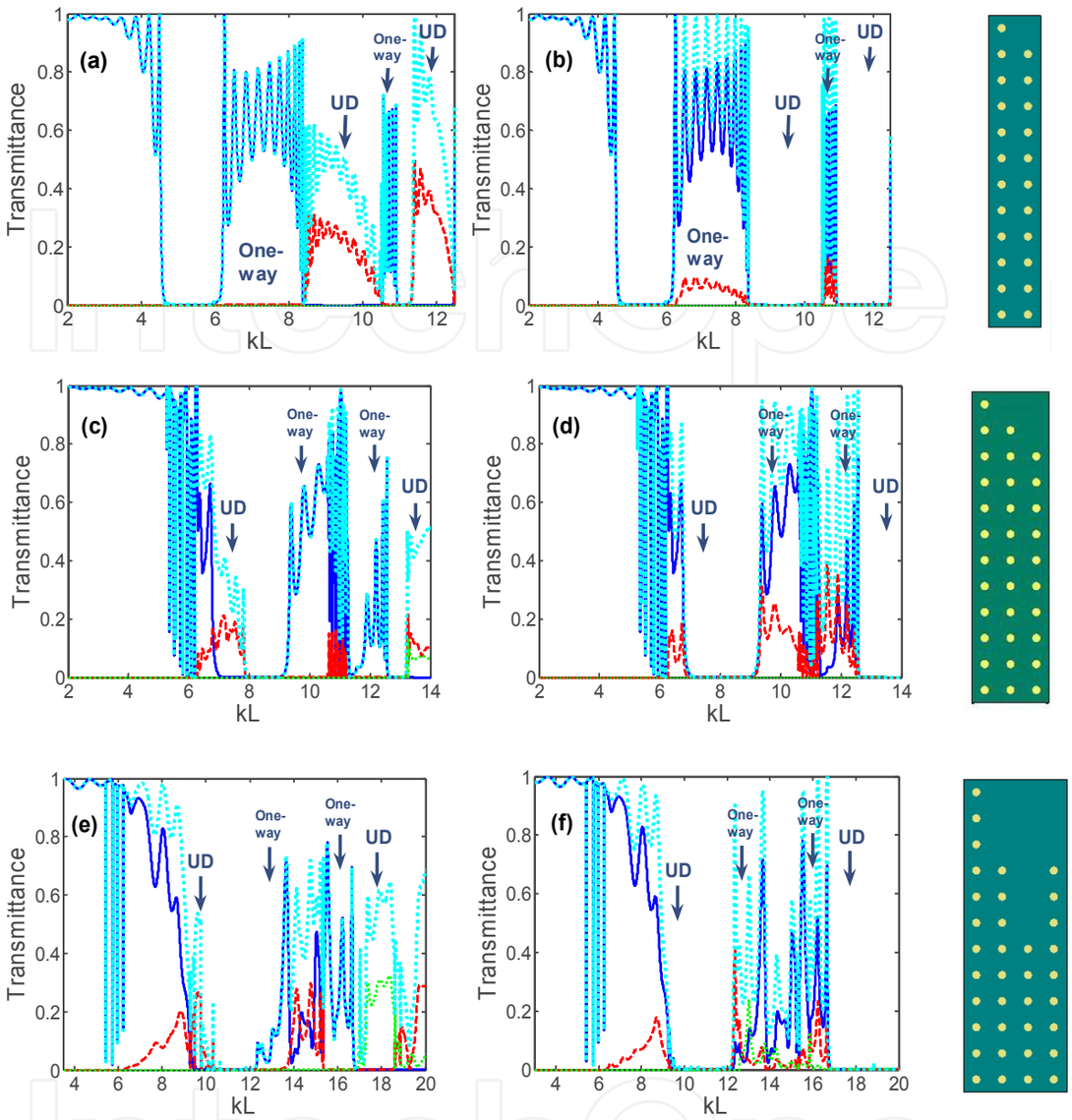

Fig. 8. Transmittance for PCGs with (a,b) L=2a, (c,d) L=3a, (e,f) L=4a, for the corrugated-side (a,c,e) and noncorrugated-side (b,d,f) illumination; d/a=0.31, $\varepsilon_r = 5.8$, Q=12, θ=0; blue solid line - t_0 ; red dashed line - $t_{\pm 1}^{\rightarrow}$ (a, e), $t_{\pm 1}^{\leftarrow}$ (b, f), $t_{-1}^{\rightarrow}$ (c), and $t_{-1}^{\leftarrow}$ (d); green dotted line - $t_{\pm 2}^{\rightarrow}$ (e), $t_{\pm 2}^{\leftarrow}$ (f), $t_{-2}^{\rightarrow}$ (c), and $t_{-2}^{\leftarrow}$ (d); cyan dotted line - $T^{\rightarrow}$ (a,c,e) and $T^{\leftarrow}$ (b,d,f); right panels – geometry of PCG within a period.

At P=4, unidirectional splitting takes place for the first (now at 9.6<kL<10.4) and third lowest Floquet-Bloch waves. - See Figs. 8(e) and 8(f). The main difference as compared to the case of P=3 is probably that the regime with $T^{\rightarrow} = t_{-2}^{\rightarrow} + t_{+2}^{\rightarrow}$ can be realized at the band edge for the third lowest Floquet-Bloch wave (at kL>16.9). It is noteworthy that one-way transmission with $T^{\rightarrow} = t_0$ and $T^{\leftarrow} > t_0$ can appear also at P>2, e.g., at 9.2<kL<10.5 in Figs. 8(c) and 8(d) and at 15.6<kL<16.9 in Figs. 8(e) and 8(f). A proper choice of the PC lattice parameters is important from the point of view of obtaining of the *switching* between

different regimes. For example, in Fig. 8(a), the ranges of $T^{\rightarrow} = t_0$ and $T^{\rightarrow} = t_{-1}^{\rightarrow} + t_{+1}^{\rightarrow}$ are adjacent but do not superimpose near kL=8.4.

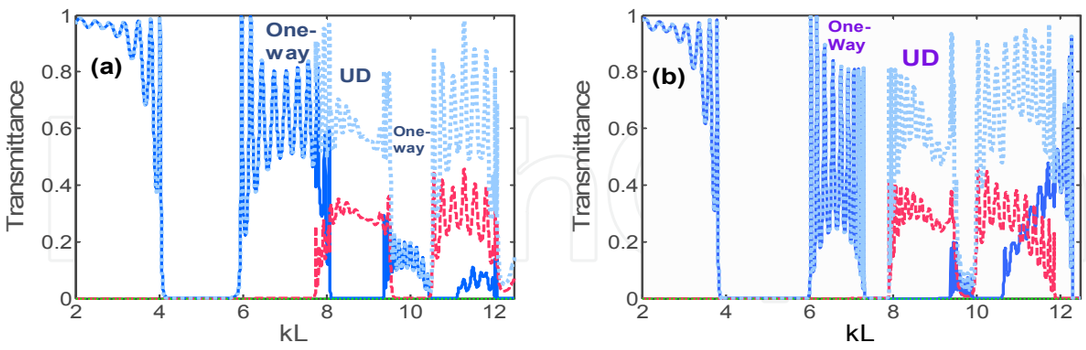

Fig. 9. Transmittance for PCGs with (a) d/a=0.4, $\varepsilon_r = 5.8$, Q=12, and (b) d/a=0.31, $\varepsilon_r = 9.61$, Q=12, at L=2a and θ=0, for corrugated-side illumination; blue solid line - t_0, red dashed line - $t_{\pm 1}^{\rightarrow}$, and blue dotted line - $T^{\rightarrow}$.

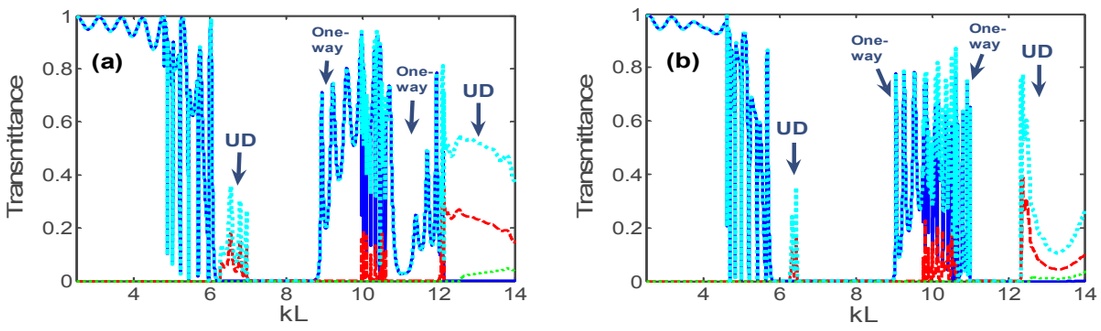

Fig. 10. Same as Fig. 9 but at L=3a, green dotted line – $t_{\pm 2}^{\rightarrow}$, cyan dotted line - $T^{\rightarrow}$.

Two more cases are shown in Figs. 9(a) and 9(b). In Fig. 9(a), the one-way and unidirectional transmission ranges superimpose at 7.7<kL<8.1. In Fig. 9(b), there is a gap between them at 7.3<kL<7.9. Hence, the PCG in Fig. 8(a) is optimal for the switching realizable by varying frequency. In Fig. 8, it has been shown that unidirectional transmission can be observed at rather small kL. Figure 10 demonstrates, in addition, that the ranges of $T^{\rightarrow} = t_0$ and $T^{\rightarrow} = t_{-1}^{\rightarrow} + t_{+1}^{\rightarrow}$ can do not superimpose at the edge of the lowest passband. Here, the corrugations are obtained by removing one rod from every two of three columns in the interface layer in Fig. 9(a) and from every third column in the interface layer in Fig. 9(b). Now, $t_{+n} = t_{-n}$ due to the used corrugation shape. Comparison of Figs. 8-10 shows that the maximal transmittance achievable in the unidirectional transmission regime for a certain higher-order Floquet-Bloch mode is strongly dependent on the PC lattice and corrugation parameters, as well as the contribution of individual higher orders.

For a PCG with fixed parameters, variation in θ gives an efficient tool for tuning. Strong modification of the transmission spectrum can be achieved even at a rather weak variation. An example is presented in Fig. 11 for the PCG illuminated from the corrugated side, for which transmittance at θ=0 is shown in Fig. 8(a). At θ=10 degrees (Fig. 11(a)), transmittance

is two-way, i.e., $t_{-1}^{\rightarrow} \neq 0$, $t_{-1}^{\leftarrow} \neq 0$, $T^{\rightarrow} > t_0$, and $T^{\leftarrow} > t_0$, for the most part of the one-way transmission range of Fig. 8(a) that belongs to the second lowest passband (here at 6.2<*kL*<8.2). At the same time, transmission remains unidirectional for the third lowest passband, but now $t_{-1}^{\rightarrow} \neq t_{+1}^{\rightarrow}$ and a stop band appears between the second and third passbands. Appearance of a narrow unidirectional transmission band in the vicinity of *kL*=5.4, where $T^{\rightarrow} = t_{-1}^{\rightarrow}$ and $T^{\leftarrow} = 0$, is probably the most interesting feature seen in Fig. 11(a). The lower boundary of this band is determined by $k=k_{-1}$ (*kL*=5.35), according to (4), so that the rapid increase of $T^{\rightarrow} = t_{-1}^{\rightarrow}$ is connected with the Rayleigh-Wood anomaly. The upper boundary is due to the narrowing and further disappearance (near *kL*=5.47) of the IFCs at increasing *kL*. The transmitted beams in this case are strongly deflected. For example, $\phi_{-1} \approx -82$ degrees at *kL*=5.4.

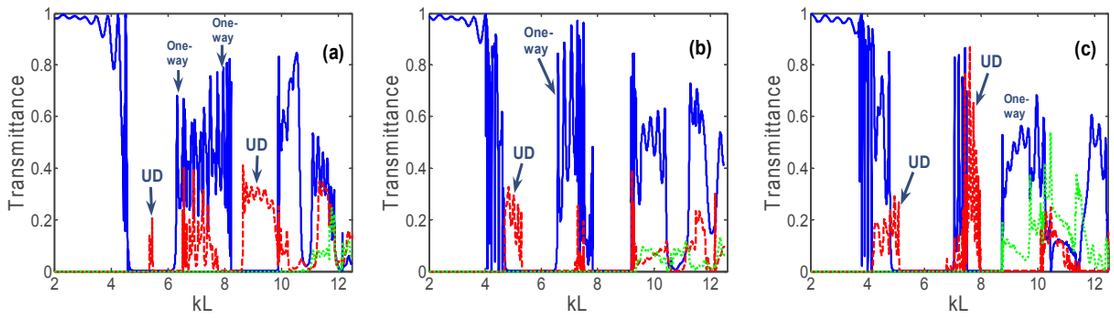

Fig. 11. Same as Fig. 8(a), but at θ=10 degrees (a), θ=20 degrees (b), and θ=30 degrees (c); blue solid line - t_0, red dashed line - $t_{-1}^{\rightarrow}$, and green dotted line - $t_{-2}^{\rightarrow}$.

Increase of θ up to 20 degrees leads to that this band becomes wider, and the switching between the regimes of $T^{\rightarrow} = T^{\leftarrow} = t_0$ (two-way, symmetric) and $T^{\rightarrow} = t_{-1}^{\rightarrow}$ (unidirectional) occurs at $kL \approx 4.7$ – See Fig. 11(b). To compare, (4) gives $k_{-1}L = 4.68$, i.e., the rapid increase of $t_{-1}^{\rightarrow}$ is again due to the Rayleigh-Wood anomaly. At the same time, the unidirectional transmission range observed in Fig. 11(a) in the vicinity of *kL*=9 disappears. The obtained results show that a rather wide range of $T^{\rightarrow} = t_{-1}^{\rightarrow}$ can appear at the edge of the lowest passband in the both unidirectional splitting (θ=0) and unidirectional deflection ($\theta \neq 0$) regimes. Further increase of θ can result in the appearance of the high-*T* unidirectional deflection range, as occurs for the second lowest Floquet-Bloch mode at *kL*=7.6 and θ=30 degrees, where $\max T^{\rightarrow} = \max t_{-1}^{\rightarrow} > 0.6$. – See Fig. 11(c). However, in this case, switching of such a kind as in Fig. 11(b) at the edge of the lowest passband cannot be obtained. Instead, there are three consequent ranges at 4<*kL*<5, which are similar to those in Fig. 8(c): $T^{\rightarrow} = t_0$ (two-way, symmetric), $T^{\rightarrow} = t_0 + t_{-1}^{\rightarrow}$ (one-way, asymmetric), and $T^{\rightarrow} = t_{-1}^{\rightarrow}$ (unidirectional). Besides, two new ranges of one-way transmission appear at 8.7<*kL*<10.1 and 11.3<*kL*<12.4, where $T^{\rightarrow} = t_0 + t_{-2}^{\rightarrow}$ and $T^{\leftarrow} = t_0 + t_{-1}^{\leftarrow} + t_{-2}^{\leftarrow}$.

Figure 12 presents the transmission spectra at the three values of θ, for the same PCG as in Fig. 9(a). The defect-mode-like unidirectional peak in Fig. 12(b) and switching between the regimes of $T^{\rightarrow} = t_0$ and $T^{\rightarrow} = t_{-1}^{\rightarrow}$ in Fig. 12(c), both being connected with the first lowest Floquet-Bloch mode, are obtained now at larger θ than in Fig. 11. Here, the rapid increase of $t_{-1}^{\rightarrow}$ has the same nature as in Fig. 11. Other features observed are similar, too. Hence, various operation regimes can co-exist in the adjacent frequency ranges, at a proper choice of the PC lattice and corrugation parameters and a value of θ.

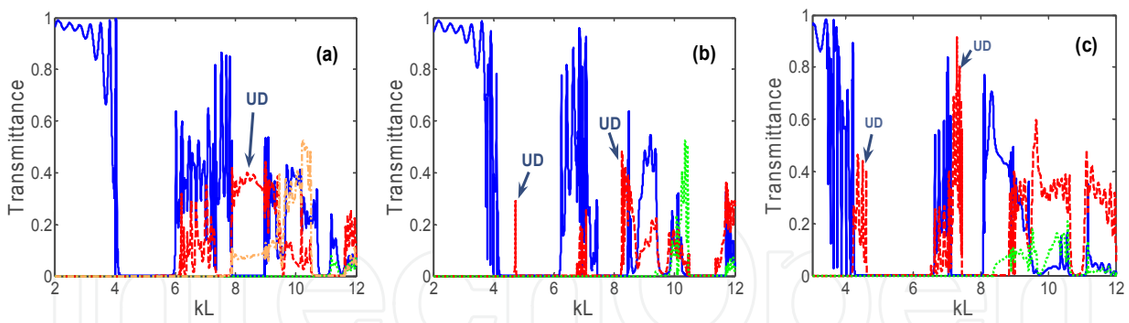

Fig. 12. Same as Fig. 9(a), but at θ=10 degrees (a), θ=20 degrees (b), and θ=30 degrees (c); blue solid line - t_0, red dashed line - $t_{-1}^{\rightarrow}$, orange dash-dotted line - $t_{+1}^{\rightarrow}$, and green dotted line - $t_{-2}^{\rightarrow}$.

There are several problems to be solved in order to design such PCGs that are consistent with the requirements and limitations regarding the realistic nanofabrication process and illumination characteristics. For example, the requirement to the frequency range of unidirectional transmission to be wide, which is connected with possible fabrication inaccuracies, should be fulfilled simultaneously with the requirement to this range to show high transmittance within a wide range of θ variation, which is important for the incident beams with a wide plane-wave angular spectrum. Figure 13 presents the transmission spectra for a PCG with the selected parameters, which is expected to better fulfil the above-mentioned requirements. The wide unidirectional transmission range with $T^{\rightarrow} = t_{-1}^{\rightarrow} > 0.8$ and $T^{\leftarrow} = 0$ is located near kL=5.6. Obtaining of θ-independent unidirectional ranges with $T^{\rightarrow} \approx 1$ should be the next step towards practical diode-type devices.

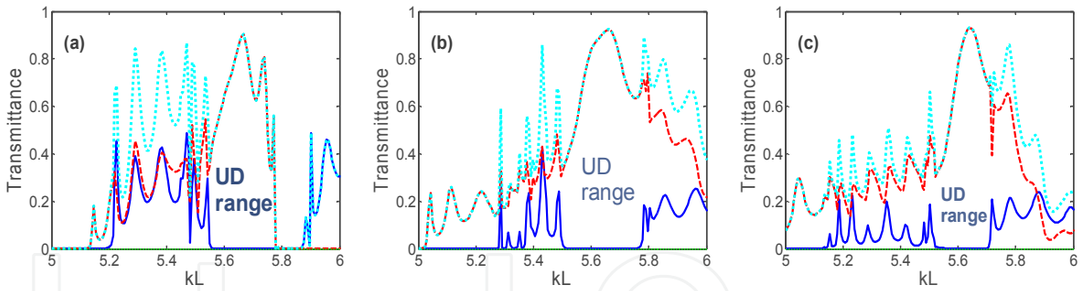

Fig. 13. Transmittance at the corrugated-side illumination for PCGs with L=2a, d/a=0.5, $\varepsilon_r = 9.61$, Q=12, θ=40 degrees (a), θ=50 degrees (b), and θ=60 degrees (c); blue solid line - t_0, red dashed line - $t_{-1}^{\rightarrow}$, cyan dotted line - $T^{\rightarrow}$.

3. Fabry-Perot type transmission

The alternating total-transmission maxima and zero-transmission minima, which can be interpreted in terms of the Fabry-Perot resonances, belong to the main features of the transmission spectra of the lossless dielectric slabs. Transmittance is given in this case by the well-known formula (Born&Wolf, 1970)

$$T = \frac{(1-\tilde{R})^2}{(1-\tilde{R})^2 + 4\tilde{R}\sin^2(N'kD\cos\theta')} \tag{9}$$

where θ' is angle of refraction, D is thickness of the slab, N' is index of refraction of the slab material, and $\tilde{R}$ is reflectance of a dielectric-air interface. The peaks of T=1 appear at $N'kD\cos\theta' = \pi m$, $m = 1,2,3,\ldots$. Fabry-Perot resonances can also appear in the noncorrugated slabs of PCs (Sakoda, 2001; Serebryannikov, 2010). In the contrast with the dielectric slabs, in PCs we have $\boldsymbol{v}_g \neq \boldsymbol{v}_{ph}$, where $\boldsymbol{v}_g$ and $\boldsymbol{v}_{ph}$ are group and phase velocity, respectively. Location of the minima and maxima of T depends, in fact, on $\boldsymbol{v}_g$. On the other hand, the *equivalent group index* can be estimated at θ=0 from the locations of the peaks of T (Sakoda, 2001):

$$N_g' = \pi c / (\Delta\omega D), \tag{10}$$

where $\Delta\omega$ is spectral distance between the neighbouring peaks. Clearly, characterization of the finite-thickness slabs of PCs in terms of N_g' is ambiguous, at least because of the unavoidable uncertainty in location of the virtual interfaces. Besides, it is assumed that $N_g' > 0$, that is not always the case. Nevertheless, this approach usually gives the estimates of N_g' that are qualitatively correct within sign, for thick slabs. Obtaining of accurate (intrinsic) values of the group index needs post-processing of the dispersion results. The corresponding formulas can be found in the literature (Foteinopoulou & Soukoulis, 2005).

In the PCGs, Fabry-Perot resonances can appear while higher orders contribute to the transmission. Since this contribution is asymmetric, i.e., dependent on the illumination side, there may be asymmetry in the appearance of the resonances, which manifests itself in a high contrast between the backward and forward transmittances. From the point of view of demonstration of such asymmetry, the regimes with nonzero transmittance in the both directions are most interesting. In particular, this is related to the one-way transmission regime with $T^{\rightarrow} = t_0$ and $T^{\leftarrow} > t_0$.

Figure 14 presents an example of strong asymmetry, which is observed in the one-way transmission regime for the fourth lowest Floquet-Bloch mode in the PCG from Fig. 9(b). Asymmetry appears here owing to that the contribution of $t_{\pm 1}^{\leftarrow}$ to $T^{\leftarrow}$ is more significant than that of t_0, while $t_{\pm 1}^{\rightarrow} = 0$. A high contrast can be achieved, e.g., $T^{\leftarrow} / T^{\rightarrow} = 11$ at $kL \approx 9.78$. Furthermore, the peaks of $T^{\leftarrow} \approx 1$ are observed, like in the case of a noncorrugated PC, or a dielectric slab. The values of N_g' obtained from (10) are given in Table 1. $k_l L$ and $k_s L$ mean the larger and smaller values of kL for each pair of the neighbouring peaks. The smaller the distance between the peaks, the larger the value of N_g' is.

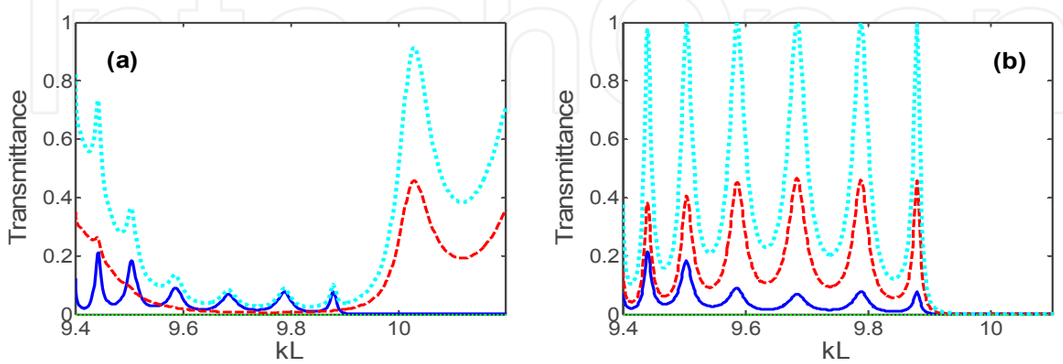

Fig. 14. Fragment of the transmission spectrum for the PCG with L=2a, d/a=0.31, $\varepsilon_r = 9.61$, Q=12, at θ=0, for corrugated-side (a) and nocorrugated-side (b) illumination; blue solid line - t_0, red dashed line - $t_{\pm 1}^{\rightarrow}$ (a) and $t_{\pm 1}^{\leftarrow}$ (b), cyan dotted line - $T^{\rightarrow}$ (a) and $T^{\leftarrow}$ (b).

	1	2	3	4	5
k_sL	9.44	9.504	9.587	9.684	9.79
k_lL	9.504	9.587	9.684	9.79	9.88
$N_g^{'}$	8.18	6.30	5.40	4.94	5.82

Table 1. Equivalent group index for the transmission peaks in Fig. 14(b).

Figure 15 illustrates the case when the same diffraction orders contribute to $T^{\leftarrow}$ and $T^{\rightarrow}$, but the contributions of individual orders strongly depend on the illumination direction. Here, two-way transmission occurs at $14<kL<15.8$, while unidirectionality with $T^{\rightarrow} \approx t_{-1}^{\rightarrow} + t_{+1}^{\rightarrow}$ takes place in the adjacent range, i.e., at $12<kL<14$. For example, the order with $n=-1$ is the main contributor at $14.1<kL<14.4$ at the noncorrugated-side illumination, but its effect tends to vanish in the vicinity of kL=14.4 at the corrugated-side illumination.

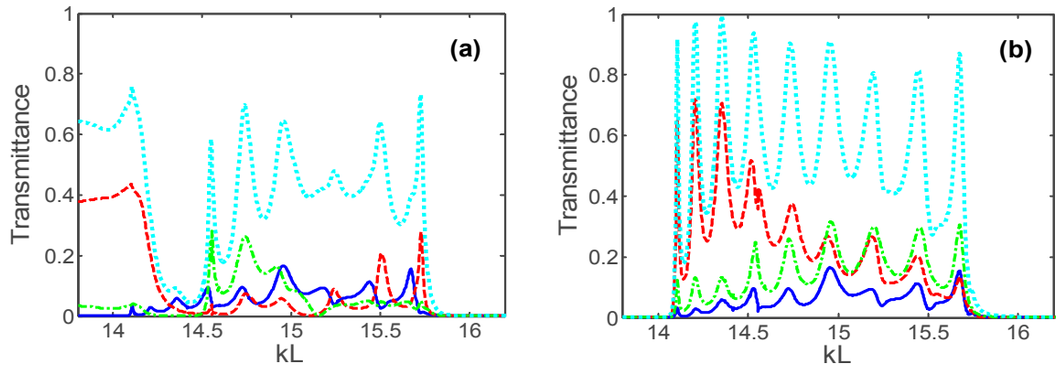

Fig. 15. Fragment of the transmission spectrum for the PCG with $L=3a$, d/a=0.4, $\varepsilon_r = 5.8$, Q=12, at θ=0, for corrugated-side (a) and nocorrugated-side (b) illumination; blue solid line - t_0, red dashed line - $t_{-1}^{\rightarrow}$ (a) and $t_{-1}^{\leftarrow}$ (b), green dash-dotted line - $t_{-2}^{\rightarrow}$ (a) and $t_{-2}^{\leftarrow}$ (b), cyan dotted line - $T^{\rightarrow}$ (a) and $T^{\leftarrow}$ (b); corrugations are the same as in Figs. 8(c) and 8(d); note that $t_{-n}^{\rightarrow} \neq t_{+n}^{\rightarrow}$ and $t_{-n}^{\leftarrow} \neq t_{+n}^{\leftarrow}$, $|n|>0$.

4. Reflection regime

Band gaps and relevant total reflections belong to the main effects known in PCs. Corrugations may lead to that the higher diffraction orders contribute to reflection starting from the frequency and kL values, which correspond to the lowest stop band of the PC. Furthermore, if corrugations are placed at one side only, reflections can be asymmetric, so that the different diffraction orders play the different roles, depending on the illumination direction, although $R^{\rightarrow} = R^{\leftarrow} = 1$. Figure 16 presents the reflection spectra for the same PCG as in Figs. 8(a) and 8(b), at θ=0. Now, $r_{\pm 1}^{\rightarrow} > 0$ at $kL>2\pi$ and $r_{\pm 1}^{\leftarrow} > 0$ at $kL>4\pi$. It is noteworthy that, in the contrast with transmission, the reciprocity principle requires that $r_0^{\rightarrow} = r_0^{\leftarrow}$ only at $kL \le 2\pi$. Hence, zero-order reflection is itself asymmetric, provided that higher order(s) are allowed to propagate in air. In fact, the possibility of contribution of higher orders to $R^{\rightarrow}$ and $R^{\leftarrow}$ mainly depends on the period of the illuminated interface, i.e., $L_1 = 2a$ and $L_2 = a$, for the corrugated and noncorrugated interfaces, respectively.

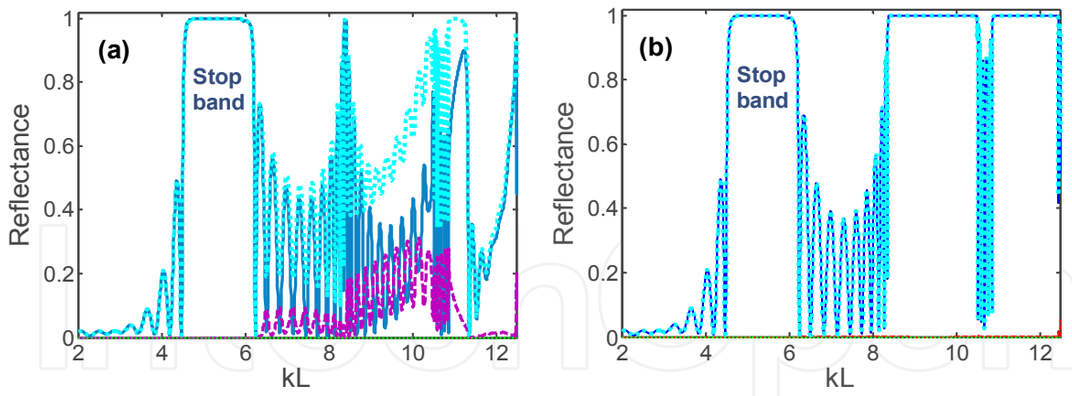

Fig. 16. Reflectance for the PCG with L=2a, d/a=0.31, $\varepsilon_r = 5.8$, Q=12, at θ=0, for (a) corrugated-side and (b) nocorrugated-side illumination; blue solid line - r_0, violet dashed line - $r_{-1}^{\rightarrow} = r_{+1}^{\rightarrow}$ (a) and $r_{-1}^{\leftarrow} = r_{+1}^{\leftarrow}$ (b), cyan dotted line - $R^{\rightarrow}$ (a) and $R^{\leftarrow}$ (b).

At P>2, some new features can be observed in the reflection spectrum as compared to Fig. 16. Figure 17 presents an example for a PCG with P=4, while the PC lattice parameters are the same as in Figs. 9(b), 10(b), and 14. Corrugations are obtained here by removing two rods from every second column, and four rods from every fourth column, so that they are similar to but not so deep as those in Figs. 8(e) and 8(f). If the corrugated side is illuminated, the orders with $n = \pm 1$ contribute to $R^{\rightarrow}$ also in the total-reflection regime at 8.5<kL<11.7. In particular, splitting with $r_0^{\rightarrow} = r_{-1}^{\rightarrow} = r_{+1}^{\rightarrow}$ and $R^{\rightarrow} = 1$ takes place at kL=9.29, 9.68, 10.54, 11.33, and 11.55. If the noncorrugated side is illuminated, zero order is the main contributor to $R^{\leftarrow}$ within the entire kL-range considered. Comparing to Fig. 16(b), the orders with $n = \pm 1$ now do not vanish but slightly contribute to $R^{\leftarrow}$ in the vicinity of kL=7 and kL=14. In these ranges, $t_{\pm 1}^{\leftarrow} \neq 0$ due to the effect of the exit (here – corrugated) interface, since higher orders may appear in $R^{\leftarrow}$ due to the input (here – noncorrugated) interface starting from kL=8π only.

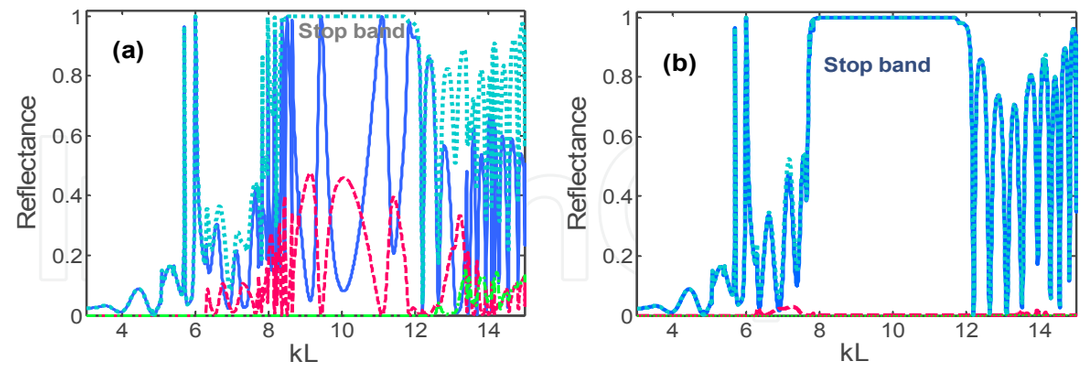

Fig. 17. Same as Fig. 16 but for L=4a and $\varepsilon_r = 9.61$; blue solid line - r_0, red dashed line - $r_{-1}^{\rightarrow} = r_{+1}^{\rightarrow}$ (a) and $r_{-1}^{\leftarrow} = r_{+1}^{\leftarrow}$ (b), green line - $r_{-2}^{\rightarrow} = r_{+2}^{\rightarrow}$ (a) and $r_{-2}^{\leftarrow} = r_{+2}^{\leftarrow}$ (b), and cyan dotted line - $R^{\rightarrow}$ (a) and $R^{\leftarrow}$ (b).

Tilting leads to that the higher orders can strongly contribute to the ranges of $R^{\rightarrow} = 1$ at smaller P than at θ=0. For example, splitting with $r_0^{\rightarrow} = r_{-1}^{\rightarrow}$ and the relatively small values of $|dr_n / d(kL)|$ can be obtained in the first stop band at P=2. Besides, the order with $n = -1$ can dominate in $R^{\rightarrow}$ at a stop band edge, where $\phi_{-1} \approx -\theta$, i.e., reflection is nearly backward.

Two examples are shown in Fig. 18. Here, $r_0^{\rightarrow} = r_{-1}^{\rightarrow}$ at kL=5.57 in Fig. 18(a), and at kL=5.66 and kL=8.29 in Fig. 18(b). Tilting can be an efficient tool of tuning in the reflection regime. Varying θ, one can change k_{-1} and, hence, obtain $r_{-1}^{\rightarrow} > 0$ for the entire, or a desired part of the lowest stop band.

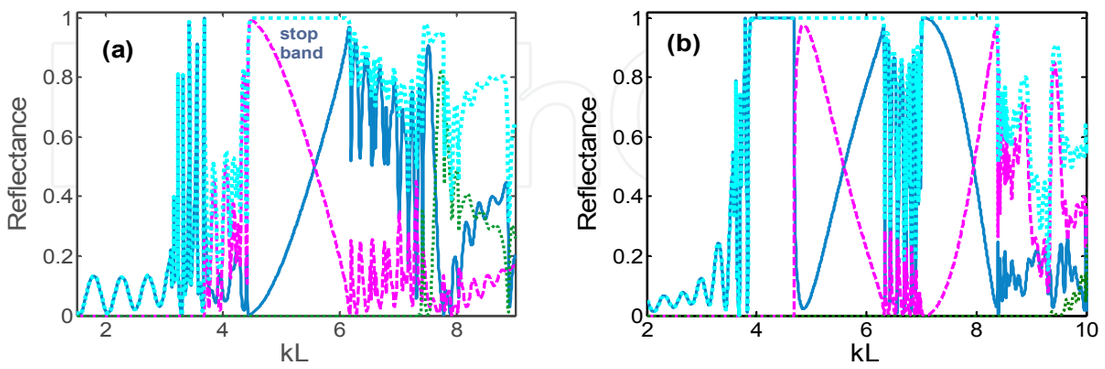

Fig. 18. Reflectance (a) for the same PCG as in Fig. 9(a) at θ=45 degrees, and (b) for the same PCG as in Fig. 9(b) at θ=20 degrees; corrugated-side illumination; blue solid line - r_0, violet dashed line - $r_{-1}^{\rightarrow}$, dark green line - $r_{-2}^{\rightarrow}$, and cyan dotted line - $R^{\rightarrow}$.

5. Conclusion

Multiple examples can be given to demonstrate that a combination of different physical phenomena can create a possibility of substantial extension of the variety of the obtainable regimes and new ideas for low-cost and/or compact designs. Thus, hybridization is a rather general approach in modern optics and physics. In this chapter, it has been shown how the effects, which are well known for the gratings, on the one hand, and those for the PCs, on the other hand, can be combined in the nonsymmetric PCGs composed of dielectric rods in such a way that new operation regimes can be obtained, which are not realizable in dielectric gratings or noncorrugated PCs. The most interesting transmission and reflection regimes of PCGs originate from the nonsymmetry, i.e., from the broken spatial inversion symmetry. The studied mechanism is characterized by absence of polarization conversion, while the extreme redistribution of the incident wave energy into that of of higher orders plays a key role. In particular, PCGs promise new solutions for unidirectional diode-like devices, splitters, deflectors, mirrors, and nano- and microwave antennas. From the point of view of the theory of PCs, introduction of corrugations while dispersion is known enables new coupling scenarios owing to diffractions. From the point of view of the grating theory, using a PC with the alternating pass and stop bands and substantially different properties of various Floquet-Bloch modes, instead of a homogeneous linear material, enables new diffraction scenarios as compared to those typical for dielectric gratings. Finally, from the point of view of the asymmetric and unidirectional transmission, PCGs demonstrate a high potential in obtaining of strong directional selectivity without breaking time reversal symmetry and, hence, without using anisotropic or nonlinear materials. A new direction in the studies of PCGs concerns asymmetric transmission for defect modes that might appear in chains of the cavity defects or/and line defects, which are parallel to the interfaces.

6. Acknowledgment

The author thanks the Deutsche Forschunsgemeinschaft for partial support of this work under Project Nos. SE1409-2/1 and SE1409-2/2, and Prof. E. Ozbay and members of his research group for fruitful discussions.

7. References

Born, M. & Wolf, E. (1970). *Principles of Optics*, Pergamon Press, Oxford

Caglayan, H.; Bulu, I. & Ozbay, E. (2008). Off-Axis Beaming From Subwavelength Apertures, *J. Appl. Phys.*, Vol. 104, No. 7, 073108

Cakmak, A.O.; Colak, E., Serebryannikov, A.E. & Ozbay, E. (2010). Unidirectional Transmission in Photonic-Crystal Gratings at Beam-Type Illumination, *Opt. Express*, Vol. 18, No. 21, pp. 22283-22298

Collardey, S.; Tarot, A.-C., Pouliguen, P. & Mahdjoubi, K. (2005). Use of Electromagnetic Band-Gap Materials for RCS Reduction, *Microwave Opt. Technol. Lett.,* Vol. 44, No. 6, pp. 546-550

Figotin, A. & Vitebsky, I. (2001). Nonreciprocal Magnetic Photonic Crystals, *Phys. Rev. E*, Vol. 63, No. 6, 066609

Foteinopoulou, S. & Soukoulis, C.M. (2005). Electromagnetic Wave Propagation in Two-Dimensional Photonic Crystals: A Study of Anomalous Refraction Effects, *Phys. Rev. B*, Vol. 72, No. 16, 165112

Gralak, B.; Enoch, S. & Tayeb, G. (2000). Anomalous Refractive Properties of Photonic Crystals, *J. Opt. Soc. Am A*, Vol. 17, No. 6, pp. 1012-1020

Hessel, A. & Oliner, A.A. (1965). A New Theory of Wood's Anomalies on Optical Gratings, *Appl. Opt.*, Vol. 4, No. 10, pp. 1275-1297

Ibrahim, S.K.; Bhandare, S., Sandel, D., et al. (2004). Non-Magnetic 30dB Integrated Optical Isolator in III/IV Material, *Electron. Lett.*, Vol. 40, No. 20, pp. 1293-1294

Inoue, K. & Ohtaka, K., Eds. (2004). *Photonic Crystals: Physics, Fabrication, and Applications*, Springer, Berlin Heidelberg New York

Joannopoulos J.D. (1995). *Photonic Crystals: Molding the Flow of Light*, Princeton Univ. Press, Princeton

Kang, X.-B.; Tan, W., Wang, Z.-S., et al. (2010). High Efficiency One-Way Transmission by One-Dimensional Photonic Crystals with Gratings on One Side, *Chin. Phys. Lett.*, Vol. 27, No. 7, 074204

Kong, J.A. (2005). *Electromagnetic Wave Theory*, EMW Publishing, Cambridge, MA

Le Thomas, N.; Houdre, R., Frandsen, L.H., et al. (2007). Grating-Assisted Superresolution of Slow Waves in Fourier Space, *Phys. Rev. B*, Vol. 76, No. 3, 035103

Li, X.-F.; Ni, X., Feng, L., et. al. (2011). Sonic-Crystal-Based Acoustic Diode, *Phys. Rev. Lett.*, Vol. 106, No. 8, 084301

Lockyear, M.J. ; Hibbins, A.P., White, K.R., and Sambles, J.R. (2006). One-Way Diffraction Gratings, *Phys. Rev. E*, Vol. 74, No. 5, 056611

Lu, W.T.; Huang, J.Y., Vodo, P. et al. (2007). A New Mechanism for Negative Refraction and Focusing Using Selective Diffraction from Surface Corrugation, *Opt. Express*, Vol. 15, No. 15, pp. 9166-9175

Luo, C.; Johnson, S.G., Joannopoulos, J.D., & Pendry, J.B. (2002). All-Angle Negative Refraction Without Negative Effective Index, *Phys. Rev. B*, Vol. 65, No. 20, 201104(R)

Magath, T. & Serebryannikov, A.E. (2005). Fast Iterative, Coupled-Integral-Equation Technique for Inhomogeneous Profiled and Periodic Slabs, *J. Opt. Soc. Am. A*, Vol. 22, No. 11, pp. 2405-2418

Nojima, S. (2007). Long-Sojourning Light in a Photonic Atoll , *J. Opt. A, Pure Appl. Opt.*, Vol. 9, No. 9, S425

Petit, R., Ed. (1980). *Electromagnetic Theory of Gratings*, Springer, Berlin Heidelberg New York

Plum, E.; Fedotov, V.A. & Zheludev, N.I. (2009). Planar Metamaterial with Transmission and Reflection that Depend on the Direction of Incidence, *Appl. Phys. Lett.*, Vol. 94, No. 13, 131901

Rüter, C.E.; Makris, K.G., El-Ganainy, R., et. al. (2010). Observation of Parity-Time Symmetry in Optics, *Nature Phys.*, Vol. 6, No. 3, pp. 192-195

Saado, Y.; Golosovsky, M., Davidov, A. & Frenkel, A. (2005). Near-Field Focusing by a Photonic Crystal Concave Mirror, *J. Appl. Phys.*, Vol. 98, No. 6, 063105

Sakoda, K. (2001). *Optical Properties of Photonic Crystals*, Springer, Berlin Heidelberg New York

Scalora, M.; Dowling, J.P., Bowden, C.M. & Bloemer, M.J. (1994). The Photonic Band Edge Optical Diode, *J. Appl. Phys.*, Vol. 76, No. 4, pp. 2023-2026

Schleuer, J. & Yariv, A. (2004). Circular Photonic Crystal Resonators, *Phys. Rev. E*, Vol. 70, No. 3, 036603

Schurig, D. & Smith, D.R. (2003). Spatial Filtering Using Media with Indefinite Permittivity and Permeability Tensors, *Appl. Phys. Lett.*, Vol. 82, No. 14, pp. 2215-2217

Serebryannikov, A.E.; Magath, T. & Schuenemann, K. (2006). Bragg Transmittance of *s*-Polarized Waves Through Finite-Thickness Photonic Crystals With Periodically Corrugated Interface, *Phys. Rev. E*, Vol. 74, No. 6, 066607

Serebryannikov, A.E. & Ozbay, E. (2009). Unidirectirectional Transmission in Nonsymmetric Gratings Containing Metallic Layers, *Opt. Express,* Vol. 17, No. 16, pp. 13335-13345

Serebryannikov, A.E. (2009). One-Way Diffraction Effects in Photonic Crystal Gratings Made of Isotropic Materials, *Phys. Rev. B*, Vol. 80, No. 15, 155117

Serebryannikov, A.E.; Ozbay, E. & Usik, P.V. (2010). Defect-Mode-Like Transmission and Localization of Light in Photonic Crystals without Defects, *Phys. Rev. B*, Vol. 82, No. 16, 165131

Shadrinov, I.V.; Fedotov, V.A., Powell, D.A., et al. (2011). Electromagnetic Wave Analogue of an Electronic Diode, *New J. Phys.*, Vol. 13, No. 3, 033025

Singh, R.; Plum, E., Menzel, C. et. al. (2009). Terahertz Metamaterial with Asymmetric Transmission, *Phys. Rev. B*, Vol. 80, No. 15, 153104

Smigaj, W. (2007). Model of Light Collimation by Photonic Crystal Surface Modes, *Phys. Rev. B*, Vol. 75, No. 20, 205430

Vodo, P.; Parimi, P.V., Wu, W.T. & Sridhar, S. (2005). Focusing by Planoconcave Lens Using Negative Refraction, *Appl. Phys. Lett.*, Vol. 86, No. 20, 201108

Wang, Z.; Chong, Y.D. & Joannopoulos, J.D. & Soljacic, M. (2008). Reflection-Free One-Way Edge Modes in a Gyromagnetic Photonic Crystal, *Phys. Rev. Lett.*, Vol. 100, No. 1, 013905

Wu, L.; Mazilu, M., Gallet, J.-F. & Krauss, T.F. (2005). Dual Lattice Photonic-Crystal Beam Splitters, *Appl. Phys. Lett.*, Vol. 86, No. 21, 211106

Yablonovitch, E. (1987). Inhibited Spontaneous Emission in Solid-State Physics and Electronics, *Phys. Rev. Lett.*, Vol. 58, No. 20, pp. 2059-2062

Yu, Z.; Wang, Z. & Fan, S. (2007). One-Way Total Reflection with One-Dimensional Magneto-Optical Photonic Crystals, *Appl. Phys. Lett.*, Vol. 90, No. 12, 121133

Yu, Z. & Fan, S. (2009). Complete Optical Isolation Created by Indirect Interband Photonic Transitions, *Nature Phot.*, Vol. 3, No. 2, pp. 91-94

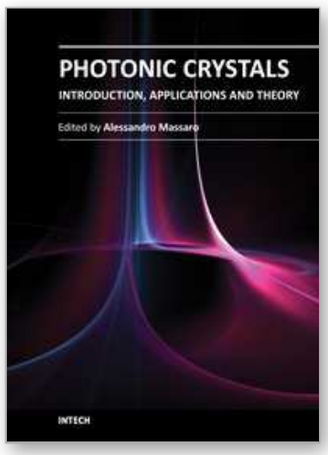

Photonic Crystals - Introduction, Applications and Theory
Edited by Dr. Alessandro Massaro

ISBN 978-953-51-0431-5
Hard cover, 344 pages
Publisher InTech
Published online 30, March, 2012
Published in print edition March, 2012

The first volume of the book concerns the introduction of photonic crystals and applications including design and modeling aspects. Photonic crystals are attractive optical materials for controlling and manipulating the flow of light. In particular, photonic crystals are of great interest for both fundamental and applied research, and the two dimensional ones are beginning to find commercial applications such as optical logic devices, micro electro-mechanical systems (MEMS), sensors. The first commercial products involving two-dimensionally periodic photonic crystals are already available in the form of photonic-crystal fibers, which use a microscale structure to confine light with radically different characteristics compared to conventional optical fiber for applications in nonlinear devices and guiding wavelengths. The goal of the first volume is to provide an overview about the listed issues.

How to reference
In order to correctly reference this scholarly work, feel free to copy and paste the following:

Andriy E. Serebryannikov (2012). Basics of the Photonic Crystal Gratings, Photonic Crystals - Introduction, Applications and Theory, Dr. Alessandro Massaro (Ed.), ISBN: 978-953-51-0431-5, InTech, Available from: http://www.intechopen.com/books/photonic-crystals-introduction-applications-and-theory/basics-of-the-photonic-crystal-gratings

INTECH
open science | open minds

InTech Europe
University Campus STeP Ri
Slavka Krautzeka 83/A
51000 Rijeka, Croatia
Phone: +385 (51) 770 447
Fax: +385 (51) 686 166
www.intechopen.com

InTech China
Unit 405, Office Block, Hotel Equatorial Shanghai
No.65, Yan An Road (West), Shanghai, 200040, China
中国上海市延安西路65号上海国际贵都大饭店办公楼405单元
Phone: +86-21-62489820
Fax: +86-21-62489821

IntechOpen